Stress-strain behavior of soils having undergone different amounts of internal erosion

S. Li & A.R. Russell
Centre for Infrastructure Engineering and Safety, School of Civil and Environmental Engineering, The University of New South Wales, Sydney, NSW 2052, Australia

D. Muir Wood
School of Science and Engineering, University of Dundee, UK

Abstract: Results of an experimental investigation are reported, conducted to study the stress-strain behavior of a soil having undergone different amounts of internal erosion. The soil used is gap-graded and cohesionless comprising silt, sand and gravel. Internal erosion tests and subsequent triaxial tests are performed in a specially designed apparatus having modified perforated end platens and a drainage system that permitted the erosion to occur. A constant water head tank is used to drive the erosion and an effluent collection system is used to observe the eroded material. Different amounts of erosion, which progressively narrow the soil grading while maintaining a constant confining stresses, are caused by passing water through compacted soil samples inside the triaxial apparatus in an upward or downward direction. Flow rate through, settlement and volume change of the samples are monitored during the erosion. After erosion, drained compression tests are conducted. Another drained compression test is also conducted on a sample that has not eroded for comparison. It is observed that drained peak deviator stresses progressively reduce and the volumetric deformation of samples become less dilative with increasing amounts of erosion.

Keywords: Internal erosion; gap-graded cohesionless soil; stress-strain behaviour; mechanical effects.

1 INTRODUCTION

Internal erosion is caused by water seeping through soils and progressively washing out particles. It is a particular concern for coheisionless soils in dam cores, filters and transition layers and silt/sand soils in dam and levee foundations. Internal erosion of the soils forming water retaining structures may occur and lead to expensive maintenance costs or, in extreme cases, total collapse. Around 50% of dam failures and dysfunctions are caused by internal erosion (Foster et al., 2000).

Recent studies have set out to investigate the mechanical influence of internal erosion on soil. Some have developed new triaxial erosion testing systems to measure the stress-strain behaviour of soils which have undergone erosion, focusing on the strength and volumetric change, initial fines content and hydraulic conductivity of the test soils (eg, Chang and Zhang, 2011; Xiao and Shwiyhat, 2012; Chang et al., 2014; Ke and Takahashi, 2012, 2014a, 2015; Sato and Kuwano, 2015; Ouyang and Takahashi, 2015). The internal erosion in these tests was allowed to occur until the effluent became clear, signifying the end of erosion. Thus the amount of erosion is not a controlled variable in those tests. Others have studied the mechanical consequences of particle removal using numerical methods, but they are not concerned with the process of coupled flow and particle removal (eg, Wood et al., 2010; Scholtès et al., 2010). In this study, a series of triaxial tests are conducted to study the stress-strain behaviour of soil samples having undergone different amounts of internal erosion. The focus is to examine the erosion characteristics in terms of flow rate and cumulative eroded soil mass, as well as the evolution of mechanical behaviour caused by the erosion.

2 TESTING APPARATUS

To study the initiation, rate of progression and consequences of internal erosion, a triaxial apparatus, modified to enable erosion, is used. The apparatus consists of a triaxial compression testing system, a drainage system enabling water to seep through samples and cause erosion, a constant head water tank to drive the seepage, and system to collect the water once it has seeped through the soil. The system is broadly similar to others (eg, Chang and Zhang, 2011; Xiao and Shwiyhat, 2012; Chang et al., 2014; Ke and Takahashi, 2012, 2014a, 2015; Sato and Kuwano, 2015; Ouyang and Takahashi, 2015). A schematic illustration is shown in Figure 2.1.

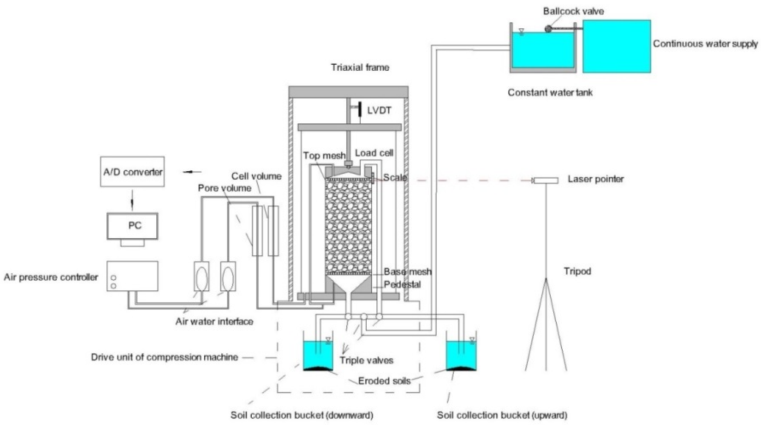

Figure 2.1. Schematic diagram of the internal erosion triaxial testing system.

2.1 Triaxial system

The triaxial testing apparatus, used to test cylindrical samples 200 mm in diameter and 400 mm in height, is displacement-controlled. A motorized load frame applies axial load to samples, in which the motor speed can provide a predetermined constant rate of displacement, and the resulting axial load can be measured by a submersible load cell at selected intervals of time. A drive unit, with a multispeed gearbox giving displacement speeds down to 0.0001 mm/min, is employed. The axial displacement of the sample during shearing is measured using a linear variable differential transducer (LVDT) with a precision of 0.0001 mm. Testing data are automatically logged at regular time intervals through a program with an interactive visual interface.

2.2 Drainage system

The base pedestal and top-cap contain funnel-shaped voids to enable seepage water containing soil particles to exit a sample through its ends and pass into a collection system. Perforated stainless steel discs cover each funnel-shaped void and provide and act as rigid base and top sample boundaries. The perforations are circular, 5 mm in diameter, and make a grid pattern with a center-to-center spacing of 8 mm. The 5 mm perforation size is sufficiently large to prevent clogging by fine particles. They are sufficiently small to prevent coarse particles from passing thus preventing collapse of a sample. The largest eroded particle is less than (and usually much less than) 15% of the maximum particle size (Wan, 2006), being 13 mm in this study. All flow channels and fittings have an internal diameter of 7.5 mm.

Seepage water can be introduced and passed through samples in both upward and downward directions to cause particle removal under a range of confining stresses and hydraulic gradients prior to shearing. Passing water through two directions enables a more homogeneous sample to be achieved prior to triaxial testing than possible by Bendahmane et al. (2008), Chang and Zhang (2011) and Ke and Takahashi (2012). In these researches, equipment permitted only the one directional passage of water causing significant variations in particle size distributions along the sample lengths.

2.3 Constant water head and effluent collection system

The seepage water is supplied via a constant head tank. The constant head tank comprises a watertight barrel fitted with an inlet ballcock valve, by which continuous water supply can be achieved. In the tests conducted here the water tank is located 3.2 m above the base of the sample, with the water exiting the sample being collected in containers level with the base, causing an average hydraulic gradient i=8 to be imposed across the sample. Higher or lower hydraulic gradients can be achieved by raising or lowering the constant head tank.

Once internal erosion is initiated, and particles begin to wash out from the sample, the flow rate and the mass of eroded soil are determined. The collected water is allowed to stand for a period of time so that suspended soil particles settle out from the water.

Axial deformation of a sample during erosion is measured by reading the vertical separation of the laser mark generated by a fixed laser pointer in front of triaxial cell.

3 TEST SOIL PREPARATION

3.1 Soil material

The soil for this study is a mixture of three base materials comprising silt, sand and gravel-sized particles in different proportions. The three base materials are referred to as silica 60G, 5 mm basalt and 10 mm basalt. The particle size distribution of each is shown in Figure 3.1. They are mixed in the proportions 0.26:0.10:0.64 to produce a gap-graded soil for testing, having a gravel content of 58.2%, with a full particle size distribution also shown in Figure 3.1. This particular gap-graded soil is selected to ensure that erosion will occur, noting that soils having gravel contents of around 60% (or larger) are internally unstable (Wan, 2006). Other physical properties of the test soil are summarized in Table 1. The erodibility of the soil mixture is evaluated as internal unstable according to several particle size distribution-based criteria (U.S. Army Corps of Engineers, 1953; Istomina, 1957; Lubochkov, 1965; Kenney and Lau, 1985, 1986; Burenkova, 1993; Wan and Fell, 2008), as shown in Table 2.

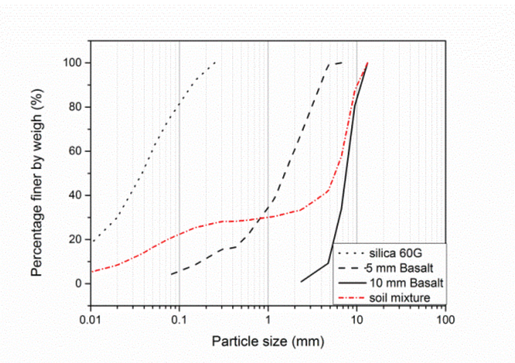

Figure 3.1. Particle size distribution of soils.

Table 1. Physical properties of the gap-graded test soil

Physical property	Value	Physical property	Value
d_{90}	10.1	$h'=d_{90}/d_{60}$	1.5
d_{60}	6.9	$h''=d_{90}/d_{15}$	232
Mean particle size d_{50}, mm	5.7	Specific gravity , Gs	2.73
d_{30}	0.97	Minimum dry density, g/cm^3	1.79
d_{15}	0.04	Maximum dry density, g/cm3	2.49
Effective particle size d_{10}, mm	0.02	USCS (ASTM D2487-11)	GM
Uniformity coefficient C_u, mm	284.6	Particle description	sub-angular
Curvature coefficient C_c	5.6	$h'=d_{90}/d_{60}$	1.5

d_x denotes the particle size finer than which the soil mass by percentage is x%

3.2 Sample formation

Moist tamping is used to form the samples as it leads to minimal particle segregation. Several thin soil layers are tamped, layer by layer, to form a sample. The modified ‘undercompaction’ method of Vo and Russell (2013) is employed to achieve samples with uniform density. The method is similar to that of Bradshaw and Baxter (2006). The compaction energy applied to each layer of soil in forming the sample is controlled in order to achieve a uniform density throughout the sample. An electric Kango percussion hammer fitted with a round steel pad with a diameter of 195 mm is used to apply compaction energy. The relationships between compacting duration and dry density for a single layer, having a moisture content of 7.3%, are obtained as shown in Figure 3.2.

Table 2. The evaluation of the mixture’s erodibility

Physical property	Value	Physical property	Value
d_{90}	10.1	$h'=d_{90}/d_{60}$	1.5
d_{60}	6.9	$h''=d_{90}/d_{15}$	232
Mean particle size d_{50}, mm	5.7	Specific gravity , Gs	2.73
d_{30}	0.97	Minimum dry density, g/cm^3	1.79
d_{15}	0.04	Maximum dry density, g/cm3	2.49
Effective particle size d_{10}, mm	0.02	USCS (ASTM D2487-11)	GM
Uniformity coefficient C_u, mm	284.6	Particle description	sub-angular
Curvature coefficient C_c	5.6	$h'=d_{90}/d_{60}$	1.5

U=unstable; P=probability of internal instability.

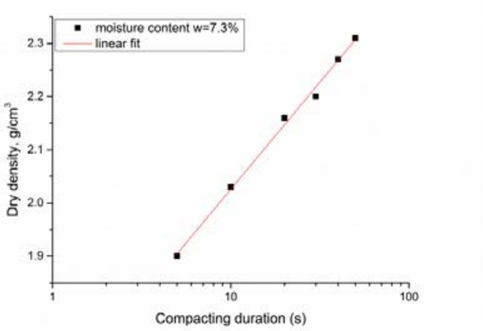

Figure 3.2. Compacting durations versus dry density of soil.

According to Skempton (1986) and Fell and Wan (2003), cohesionless soils compacted to a relative density greater than 65% have a low likelihood of internal erosion. In this study, all the samples are prepared targeting a density of 2.08 g/cm^3 when the moisture content is 7.3%, which corresponds to a relative density of 50%. The corresponding compacting duration for a single layer to reach the target is 14.5 s. Compaction trials on a layered soil showed that, when the top layer was subjected to 14.5 seconds of compaction, the top layer absorbed 75% of compaction energy, the second layer absorbed 20% of the compaction energy and the bottom layer absorbed 5% of the compaction energy. It follows, using the Vo and Russell (2013) technique, that the compaction times for each layer of a six layered sample are 14.5, 14.5, 14.5, 14.3, 14.0, 20.0s, (from bottom to top) will produce a sample with a dry density of 2.08 g/cm^3 throughout. The uniformity of the density of a sample was checked by measuring the thickness of each layer. The maximum, minimum and average ratios between actual density and target density are 1.08, 0.99 and 1.03, respectively,

4 TEST PROCEDURES

The purpose of this experimental investigation is to study the erosion characteristics of a gap-graded silt-sand-gravel mixture and its mechanical response following different amounts of internal erosion.

4.1 Saturation, consolidation and erosion

A sample is placed in the triaxial cell and then saturated to achieve a B-value of at least 0.95. It is then consolidated under an isotropic confining stress of 50 kPa. An erosion test is then performed.

A hydraulic gradient of i=8 is sufficient to cause fine particles to migrate and the samples to erode internally. A confining pressure of 80 kPa is applied during erosion. As the constant head tank imposes a pore water pressure of about 30 kPa where it enters a sample, and the water pressure is 0 kPa where it exits the sample, a gradient of effective stress exists across the sample as erosion occurs, with maximum and minimum values of about 80 kPa and 50 kPa.

Three different samples are subjected to three different amounts of erosion by passing through 15, 45 or 90 litres of water. The time required for the collected effluent to reach certain volumes is recorded. The seepage direction is reversed after every 15 liters of seepage, causing the effective stress gradients to be reversed also.

The changes in volume of the samples during erosion are determined using the cell volume changes, and the axial settlements are measured using the laser pointer.

Once the required volume of water had passed through each sample the confining pressure is raised to 260 kPa and the pore pressure is raised to 210 kPa, imposing a uniform and isotropic effective stress of 50 kPa on each sample, immediately prior to conducting a drained triaxial compression test.

4.2 Drained triaxial compression tests

Drained triaxial compression tests are conducted at a strain rate of 0.2 mm/min on the samples subjected to different amounts of internal erosion as well as a sample which had not been subjected to internal erosion. This strain rate was determined to be sufficiently slow for drained conditions to prevail. The confining and pore pressures are maintained constant at 260 kPa and 210 kPa, respectively. The axial displacement and axial load are automatically recorded every 20 seconds and photographs of the pore volume and cell volume burettes are captured using a high definition camera every 60 seconds.

5 RESULTS AND DISCUSSION

5.1 Internal erosion results

The flow rate is used here as an indicator of the progress of internal erosion. Richards and Reddy (2009) suggest that hydraulic velocity is a better indicator than flow rate for cohesionless soils. However, since the true cross-sectional area of seepage flow in a sample is not measured here, it was not possible to determine the hydraulic velocity in a reliable way.

The variations of flow rate and volumetric strain with time for the sample subjected to 90 liters of seepage are shown in Figure 5.1. The flow rate generally increases with time until a certain time is reached, beyond which it becomes stable. The increasing flow rate suggests that fine particles are being removed creating additional void space. At a certain time, once a large amount of fine particles have been removed, stable flow channels have formed within the sample and a stable flow rate is observed. The soil sample reduced in volume at all times, albeit it by very small amounts, and the reduction is most pronounced during the initial stages when particle removal is most prevalent.

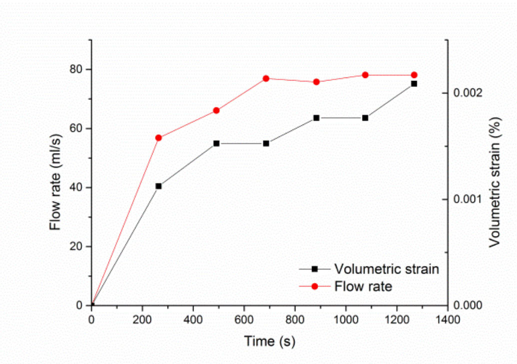

Figure 5.1. Flow rate and volumetric strain with time.

5.2 Post-erosion particle size distributions

After erosion and the subsequent triaxial test each sample is quartered using four layers of equal thickness. The particle size distribution of each is determined and those for the sample subjected to 90 liters of seepage are shown in Figure 5.4. The bottom quarter erodes the most while the top quarter erodes the least. The second and third quarters experience the same amount of erosion. Although the variation in post-erosion grading at top and bottom layers cannot really be eliminated because of gravity and the physical structure of gap-graded soil, the post-erosion grading at middle part of sample shows an uniform erosion.

5.3 Drained compression test

Drained tests are conducted on samples subjected to 15, 45 and 90 litres of seepage, along with a sample which had not been subjected to erosion. A repeat test on a sample subjected to 45 liters seepage was also conducted. Figure 5.4 plots the stress-strain curves together with the volumetric strain curves. Table 3 presents the friction angles and the dilation angles of each sample at peak and large strains. These friction angles are obtained by assuming zero cohesion.

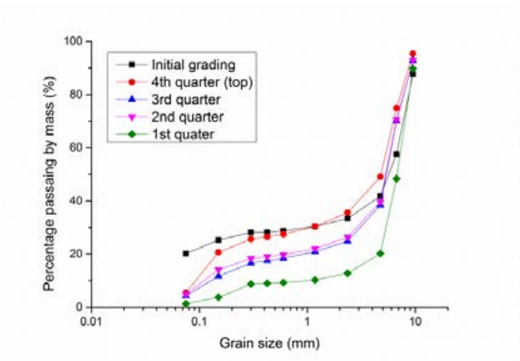

Figure 5.4. Post-erosion particle size distribution.

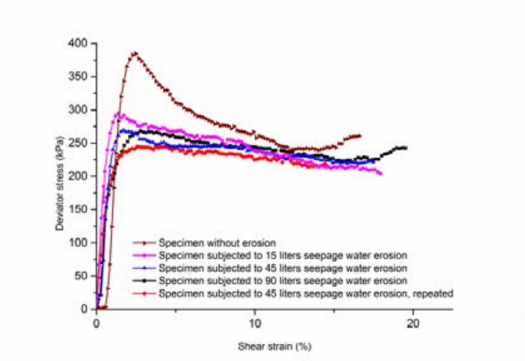

(a) Stress-strain relationships.

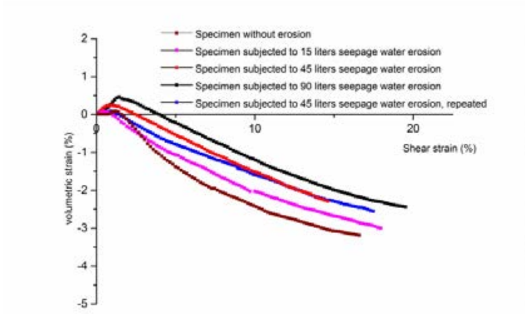

(b) Volumetric strain and shear strain relationships.
Figure 5.5. Drained compression tests on samples subjected to different amount of erosion.

The drained peak strength of the eroded samples is significantly lower than that of the sample which had not experienced erosion, in agreement with Wood et al. (2010), Ke and Takahashi (2014) and Chang et al. (2014).

The peak deviator stress tends to decrease as the volume of seepage water and erosion increase. The rate at which the strength decrease occurs tends to slow down as the volume of seepage water increases. This is consistent with the slow-down of the rate of eroded soil mass accumulation.

The large-strain shear strengths exhibited a different trend. The sample which experienced the most erosion (from 90 litres of seepage) has a larger strength than those which experienced lesser erosion (from 15 and 45 litres of seepage). At large strains, where the initial (post-erosion) sample density is not expected to affect the large strain strength, the increasing coarseness of particle size distribution following erosion may be the cause for the strength increase. This trend is consistent with findings by Chang et al. (2014). However, the increasing coarseness of the particle size distributions of the eroded samples does not explain why they had lesser constant volume strengths than the sample which had not experienced erosion. Further data is needed to explore and confirm this aspect of behavior and understand its causes.

As can be seen in Figure 5.2(b) the volumetric deformations of samples became less contractive at small shear strains with increasing amounts of erosion. Also, at large shear strains the samples subjected to erosion exhibited a reduced tendency for dilation compared to the sample which had not experienced erosion. The erosion caused the samples to become looser and thus tend to be more contractive at large shear strains, in agreement with Scholtes et al. (2010) and Chang and Zhang (2011).From Table 3, the friction angles and the dilation angles at peak are greater than each of them at large strain. And generally, the friction angle and dilation angle at peak slightly reduces as erosion proceeds, while the differences in friction angles at large strain is minor. For eroded soils, the differences in dilation angles at large strain are not much.

Table 3. The change in friction angle of samples subejected to different amounts of erosion

Amount of erosion (litres)	Percentage of lost fine particles occupies total mass	Peak friction angle (°)	Large strain friction angle(°)	Dilation angle at peak (°)	Dilation angle at large strain (°)
0	0	50.1	43.8	25.1	2.3
15	4.6%	47	43	20.8	5.7
45	7.1%	46.7	43.5	10.2	6.3
90	7.7%	46.3	43.8	13.5	5.7

4. CONCLUSIONS

An experimental investigation was conducted to study the erosion progression and the post-erosion stress-strain behavior of a gap-graded silt-sand-gravel mixture. During erosion the flow rate gradually increased prior to attaining a constant value. In the drained triaxial compression tests it was observed that the peak deviator stresses progressively reduced with increasing amounts of erosion, due to the samples becoming progressively looser with increasing amounts of erosion. The samples became less dilative with increasing amounts of erosion, again due to the samples becoming progressively looser with increasing amounts of erosion. For the eroded samples the large strain shear strengths tended to increase with the amount of erosion, probably caused by the increasing coarseness of the particle size distributions. In contrast, the eroded samples had lesser constant volume strengths than the sample which had not experienced erosion. Microstructural investigation like x-ray CT test is needed to explore and confirm the mechanism of the macro-behavior and understand its causes.

REFERENCES

Bendahmane, F., Marot, D., and Alexis, A. (2008). "*Experimental parametric study of suffusion and backward erosion*," *Journal of Geotechnical and Geoenvironmental Engineering*, 134(1), 57-67.

Bradshaw, A.S., and Baxter, C.D.P. (2007). "*Sample preparation of silts for liquefaction testing*," *Geotechnical Testing Journal*, 30(4), 324-332.

Burenkova, V.V. (1993). Assessment of suffusion in non-cohesive and graded soils. Filters in geotechnical and hydraulic engineering. Balkema, Rotterdam, 357-360.

Chang, D.S. and Zhang, L.M. (2011). "*A Stress-controlled Erosion Apparatus for Studying Internal Erosion in Soils*," Geotechnical Testing Journal, 34(6), 579-589.

Chang, D., Zhang, L., & Cheuk, J. (2014). *Mechanical consequences of internal soil erosion*. HKIE Transactions, 21(4), 198-208.

Fell, R., Wan, C.F., Cyganiewicz, J., and Foster, M. (2003). "*Time for development of internal erosion and piping in embankment dams*," *Journal of geotechnical and geoenvironmental engineering*, 129(4), 307-314.

Foster, M., Fell, R. and Spannagle, M. (2000). "*The statistics of embankment dam failures and accidents. Can*," Geotech. J., 37:1000-1024.

Istomina, V.S., (1957). Filtration Stability of Soils, Gostroizdat, Moscow.

Ke, L. and Takahashi, A.(2014) "Triaxial Erosion Test for Evaluation of Mechanical Consequences of Internal Erosion," Geotechnical Testing Journal, 37(2), 347-364.

Ke, L., and Takahashi, A. (2012). "Strength reduction of cohesionless soil due to internal erosion induced by one-dimensional upward seepage flow," *Soils and Foundations*, 52(4), 698-711.

Ke, L., and Takahashi, A. (2015). "Drained monotonic responses of suffusional cohesionless soils," *Journal of Geotechnical and Geoenvironmental Engineering*, 141(8), 04015033.

Kenney, T.C., and Lau, D. (1985). "*Internal stability of granular filters*," *Canadian geotechnical journal*, 22(2), 215-225.

Kenney, T.C., and Lau, D. (1986). "*Internal stability of granular filters: Reply*," *Canadian Geotechnical Journal*, 23(3), 420-423.

Ladd, R.S. (1978) "*Preparing test specimens using undercompaction*," *Geotechnical Testing Journal*, 1(1), 16-23.

Lubochkov, E.A. (1965). "*Graphical and analytical methods for the determination of internal stability of filters consisting of non cohesive soil*," Izvestia, vniig, 78, 255-280.

Ouyang, M., and Takahashi, A. (2015). "*Influence of initial fines content on fabric of soils subjected to internal erosion*," *Canadian Geotechnical Journal*, 53(2), 299-313.

Richards, K.S., and Reddy, K.R. (2009). "True triaxial piping test apparatus for evaluation of piping potential in earth structures," *Geotechnical Testing Journal*, 33(1), 1-13.

Sato, M., and Kuwano, R. (2015). "Influence of location of subsurface structures on development of underground cavities induced by internal erosion", *Soils and Foundations*, 55(4), 829-840.

Scholtès, L., Hicher, P.Y., and Sibille, L. (2010). "*Multiscale approaches to describe mechanical responses induced by particle removal in granular materials*," *Comptes Rendus Mécanique*, 338(10-11), 627-638.

U.S. Army Corps of Engineers, (1953). "*Filter Experiments and Design Criteria*," Technical Memorandum No. 3-360, Waterways Experiment Station, Vicksburg, MS.

Vo, T., and Russell, A.R. (2013). "*Unsaturated soil interacting with a rotating model wall*" *International Journal of Physical Modelling in Geotechnics*, 13(2), 63-78.

Wan, C.F., and Fell, R. (2008). "*Assessing the potential of internal instability and suffusion in embankment dams and their foundations*," *Journal of Geotechnical and Geoenvironmental Engineering*, 134(3), 401-407.

Wan, C.F. (2006). *Experimental investigations of piping erosion and suffusion of soils in embankment dams and their foundations*. *PhD thesis*. The University of New South Wales, Sydney, Australia.

Wood, D.M., Maeda, K., and Nukudani, E. (2010). "*Modelling mechanical consequences of erosion*," *Geotechnique*, 60(6), 447-457.

Xiao, M., and Shwiyhat, N. (2012). "*Experimental investigation of the effects of suffusion on physical and geomechanic characteristics of sandy soils*," *Geotechnical Testing Journal*, Vol. 35, No. 6, 2012, pp. 890-900.